Novel Methods for Characterization of Paroxysmal Atrial Fibrillation in Human Left Atria

Jichao Zhao[1*], Yan Yao[2,#], Wen Huang[2], Rui Shi[2], Shu Zhang[2], Ian J. LeGrice[1,5], Nigel A. Lever[1,3,4] and Bruce H. Smaill[1,5]

[1]*Auckland Bioengineering Institute, University of Auckland, Auckland, New Zealand*

[2]*Clinical EP Laboratory and Arrhythmia Center, Fu Wai Hospital and Cardiovascular Institute, Peking Union Medical College and Chinese Academy of Medical Sciences, Beijing, China*

[3]*Greenlane Cardiovascular Services, Auckland City Hospital, New Zealand*

[4]*Medicine Department, Auckland, New Zealand*

[5]*Physiology Department, University of Auckland, Auckland, New Zealand*

Abstract: *Introduction:* More effective methods for characterizing 3D electrical activity in human left atrium (LA) are needed to identify substrates/triggers and microreentrant circuit for paroxysmal atrial fibrillation (PAF). We describe a novel wavelet-based approach and wave-front centroid tracking that have been used to reconstruct regional activation frequency and electrical activation pathways from non-contact multi-electrode array.

Methods: Data from 13 patients acquired prior to ablation for PAF with a 64 electrode noncontact catheter positioned in the LA were analysed. Unipolar electrograms were reconstructed at 2048 locations across each LA endocardial surface. Weighted fine- and coarse-scale electrograms were constructed by wavelet decomposition and combined with peak detection to identify atrial fibrillation (AF) activation frequency and fractionated activity at each site. LA regions with upper quartile AF frequencies were identified for each patient. On the other hand, a wave-front centroid tracking approach was introduced for this first time to detect macro-reentrant circuit during PAF.

Results: The results employing wavelet-based analysis on atrial unipolar electrograms are validated by the signals recorded simultaneously via the contacted ablation catheter and visually tracking the 3D spread of activation through the interest region. Multiple connected regions of high frequency electrical activity were seen; most often in left superior pulmonary vein (10/12), septum (9/12) and atrial roof (9/12), as well as the ridge (8/12). The wave-front centroid tracking approach detects a major macro circuit involving LPVs, PLA, atrial floor, MV, septum, atrial roof and ridge. The regions with high frequency by wave-front tracking are consistent with the results using wavelet approach and our clinical observations.

Conclusions: The wavelet-based technique and wave-front centroid tracking approach provide a robust means of extracting spatio-temporal characteristics of PAF. The approach could facilitate accurate identification of pro-arrhythmic substrate and triggers, and therefore, to improve success rate of catheter ablation for AF.

Keywords: Atrial fibrillation, Paroxysmal atrial fibrillation, Substrate detection, Activation frequency, Non-contact mapping, Unipolar electrograms.

1. INTRODUCTION

Atrial fibrillation (AF) is common in the elderly and is associated with a range of clinical conditions including hypertension, valvular disease and heart failure. AF leads to diminished quality of life, and increased morbidity and mortality [1]. Percutaneous radiofrequency catheter ablation is widely used to treat patients with AF and the procedure is still evolving. The most common AF ablation techniques are pulmonary vein (PV) isolation and ablation guided by identifying specific substrates that may give rise to reentrant arrhythmia. The latter include regions with complex fractionated atrial electrograms (CFAEs) [2] or regions with high fibrillation frequency that are generally identified using Fourier analysis [3]. Nowadays, with paroxysmal AF (PAF), the use of catheter ablation to isolate the PVs has an 80% success rate. However, it appears different research centers worldwide employ different ablation strategies and tools [4], it is still not clear how to optimize ablation procedure and reduce the number of procedures per patient. The fundamental reason is that we lack accurate information on AF substrates/triggers and marco-reentrant circuit in PAF patients.

*Address correspondence to this author at the Auckland Bioengineering Institute, University of Auckland, Auckland, 1142, New Zealand;
Tel: (00)64-9-3737599; Ext 86505; Fax: (00)64-9-3677157;
E-mail: j.zhao@auckland.ac.nz
#Both authors contribute equally

Identification of critical regions of PAF with conventional contact mapping technologies based on point-by-point sequential acquisition suffers from several problems including being time consuming, lacking flexibility, as well as the difficulty of assessing temporal electrical variation. The non-contact mapping system (Ensite 3000, St Jude Medical) [5] allows automatic generation of isopotential maps of a left atrium (LA) from a single beat by the simultaneous reconstruction of up to 3,600 virtual endocardial electrograms, which are crucial for studying the electropathology PAF. The non-contact mapping has been widely validated in many previous studies [6]. However, the unipolar signals generated by the non-contact mapping are aproned to noise (especially QRS from ventricles), and have varying waveform morphology, how to accurately interpret the atrial electrograms is challenging.

The purpose of this study is twofold. Firstly, we developed a robust method, a wavelet filter, to systematically determine activation frequency of atrial unipolar electrograms across LA in PAF patients. It will illustrate the exact triggers/substrates of PAF. Secondly, we proposed a novel approach to detect major electrical pathways in atrial chambers. The ultimate goal of this study is to guide catheter ablation with PAF patients more effectively by providing accurate information on substrates of AF.

2. METHODS

2.1. Data Acquisition

A decapolar 6F electrode catheter (Daig, St Jude Medical, St Paul, MN) was positioned in the coronary sinus [7]. A 9F multiple electrode array catheter was placed in the middle of the LA via a transseptal approach with the support of a supersiff guide wire (Biosense Webster, Diamond Bar, CA) and with the J tip placed in the left superior pulmonary vein (PSPV). An 8 mm tip deflectable ablation catheter (Bard Electrophysiology, Lowell, MA or St Jude Medical, Irvine CA) was then introduced into the LA via a second transseptal puncture. Intravenous heparin was administered after transseptal puncture to maintain an activated clotting time of 300-350 seconds during the procedure. LA endocardial geometry was acquired and noncontact maps were then recorded for 4 to 8 seconds using the EnSite 3000 system (St Jude Medical, St Paul, MN: Sampling rate 1200 Hz; bandwidth 2-600 Hz; sensitivity10 μV) following which, stepwise-linear ablation procedures were undertaken for patients with PAF. LA geometry information and all electrical recording data at 2048 locations were exported and processed using custom-written Matlab (7.1, The Mathworks Inc., Natick, MA, 2010) applications. Atrial endocardial surface is displayed at anterior and posterior views respectively in Fig. (**1A**). Here, original atrial unipolar electrograms at four sites are shown from the LA (Fig. **1B**): site I is in the anterior wall of LA, II is from the atrial roof, III the left superior pulmonary vein (LSPV) sleeve, and IV the posterior LA (PLA).

2.2. Wavelet Filtering and Activation Frequency

Wavelet transformation was introduced two decades ago by Daubechies [8]. Nowadays, wavelet transform analysis has been applied to a wide variety of biomedical signals [9], e.g., the body surface ECG [10]. The reason makes wavelet method especially valuable is that its unique ability to elucidate simultaneously both local spectral and temporal information from a signal in a more flexible way than any other approach, e.g., the fast Fourier transform (FFT). Furthermore, it offers an option to manipulate electrograms by combining different components of frequency bands in order to filter out noise. We have used wavelet filtering to identify cycles of coordinated local atrial activation as distinct from decoupled local activity as a result of wavefront collision, or as a result of far field electrical activity.

In this work, we chose to employ continuous wavelet transform W, which is defined as:

$$Wf(\tau.s) = \frac{1}{\sqrt{|s|}} \int_{-\infty}^{+\infty} f(t)\Psi\left(\frac{t-\tau}{s}\right)dt$$

And f is the unipolar electrograms, (t) is the first derivative of a Gaussian wavelet. Fig. (**2A-B**) display the Gaussian function and its derivative $\psi(t)$, respectively. τ is the location parameter of the wavelet and s is the dilation parameter of the wavelet. The value of the dilation parameter s ranges from 1 to 30.

Here, we selected a simple function $sin(t)$ and $f = sin(t)+$ *random noise* to illustrate the basic idea of wavelet approach (blue and red lines in Fig. (**2C-I**), respectively). After applying wavelet transform on f, Wf gives the scalogram, i.e., the two-dimensional wavelet energy density function (Fig. **2C-II**). Here, the y-axis denotes for the dilation parameter s. The yellow-white color in the density function indicates a decrease in signal value $f(t)$, and red-black suggests increased value. The six 1D functions along $s=5, 10, 15, 20, 25, 30$ in the scalogram were plotted in Fig. (**2C-III**-**2C-VIII**), respectively. We can see that the larger value of s corresponds to lower frequency in the 2D energy function. We constructed fine and coarse scale electrograms f_{fine} and f_{coarse} by weighted top seven fine scales ($s = 1..7$) and bottom seven coarse scales ($s = 24..30$) in the scalogram, displayed in Fig. (**2C-IX** and **2C-X**), respectively. Clearly, f_{fine} captures all local activations, which we will use to analyze fractionation of atrial electrograms; f_{coarse} reflects the energy release and retention, which we employ to detect atrial activation time. Weighted fine and coarse scale electrograms f_{fine} and f_{coarse} were constructed as follows:

$$f_{fine}(t) = \frac{\sum_{s=1}^{7} Wf(t.s)E_{fine}(s)}{\sum_{s=1}^{7} E_{fine}(s)}$$

where the weight factors $E_{fine}(s)$ are defined as follows:

$$E_{fine}(s) = e^{-0.061(i-1)^2}$$

here i from 1 to 7, respectively for $s = 1$ to 7, and similarly we can define f_{coarse} and $E_{coarse}(s)$.

Next, we take atrial electrograms at site I in Fig. (**1B-I**) to demonstrate how we employ wavelet analysis to estimate activation frequency. Fig. (**3**) A-B display ECG I and ECG aVF leads during the same time when unipolar signals were recorded. To study atrial electrograms properly, ventricular activities (with comparatively larger magnitude) have to firstly be handled with care. There exist a range of methods to subtract ventricular signals using the standard 12-lead surface ECG data [11, 12] recorded simultaneously. These methods
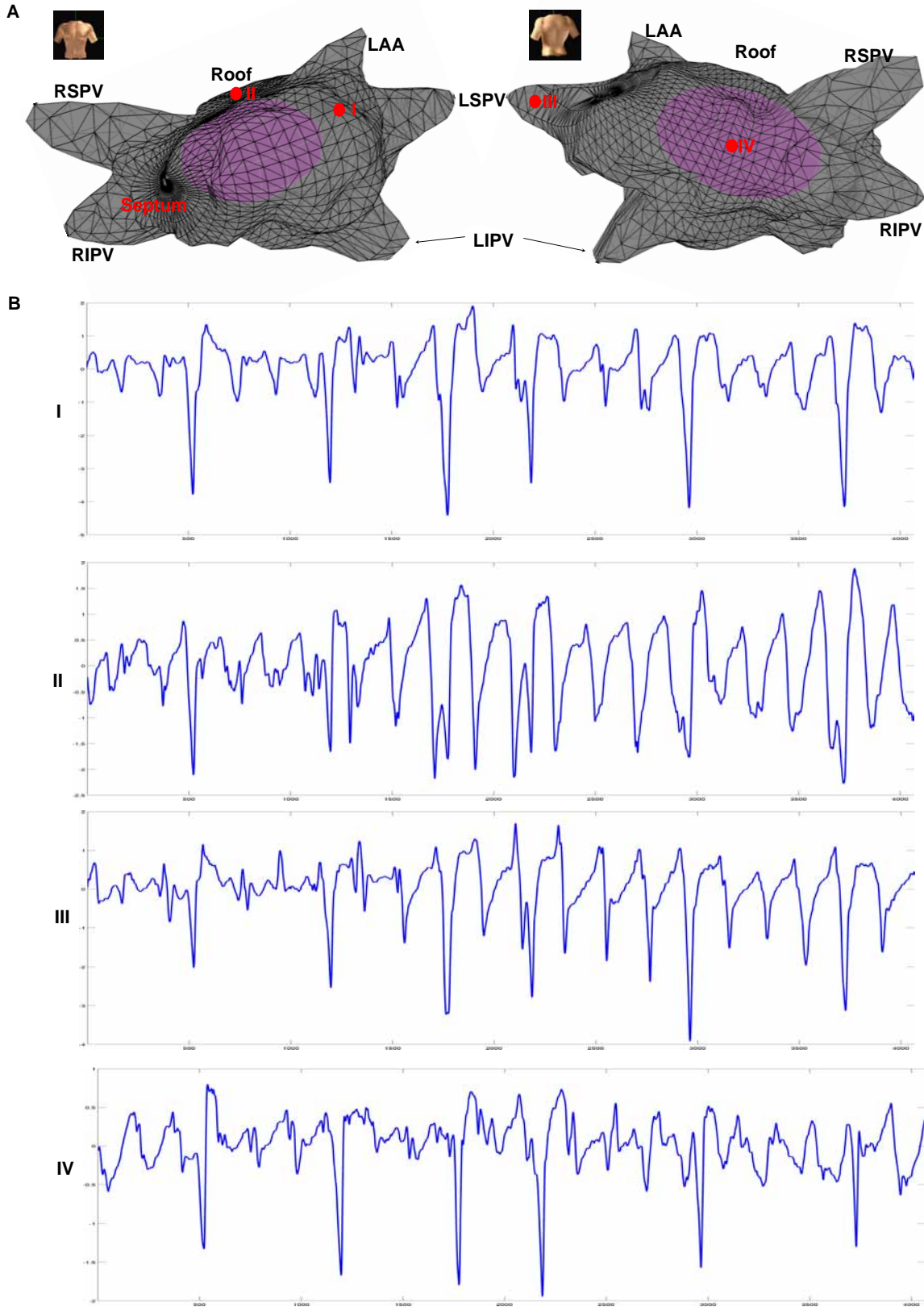
Fig. (1). 3D reconstruction atrial endocardial surface and four typical virtual electrograms reconstructed from multi-electrode noncontact array recordings in the left atrium (LA) of one patient with paroxysmal atrial fibrillation (PAF). (**A**) Anterior and posterior views of 3D LA endocardial surface reconstructed during mapping. (**B**) Typical unipolar electrogram at four sites I-IV, in vicinity of anterior wall, atrial roof, LSPV sleeve, and posterior LA (PLA), respectively. RSPV, right superior pulmonary vein; RIPV, right inferior pulmonary vein; LSPV, left superior pulmonary vein; LIPV, left inferior pulmonary vein; LAA, left atrial appendage.
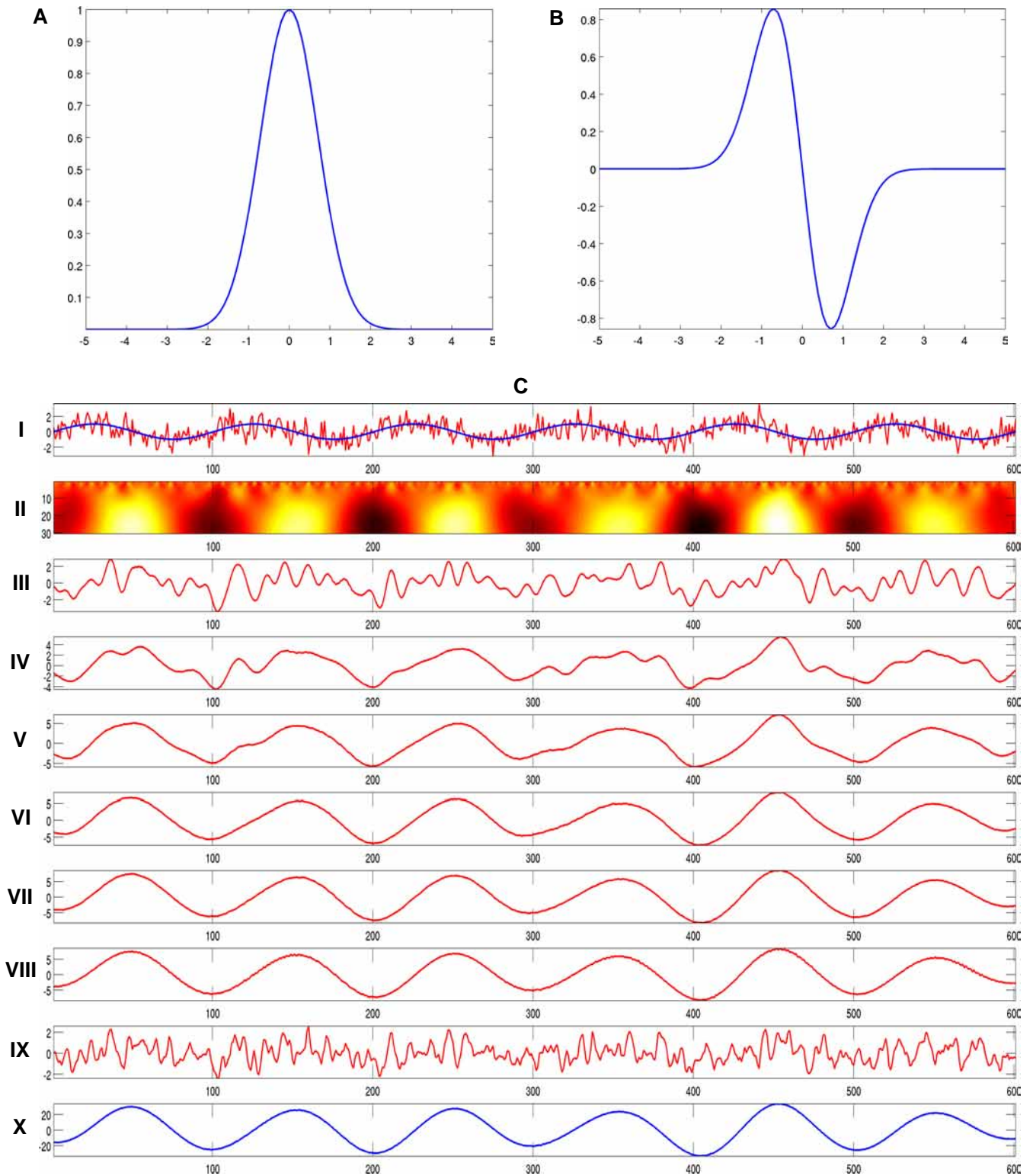
Fig. (2). Wavelet method and its illustration on a simple function. (**A**) Gaussian wavelet. (**B**) $\Psi(t)$, first derivative of a Gaussian function. (**C**) The wavelet decomposition of the function $f = sin(t) + random\ noise$. $sin(t)$ and $f = sin(t) + random\ noise$ were plotted in **I**, the scalogram Wf in **II** and the six 1D functions along $s=5, 10, 15, 20, 25, 30$ in the scalogram were plotted in **III** - **VIII**, respectively. Reconstructed fine and coarse scale electrograms f_{fine} and f_{coarse} in **IX** and **X**.
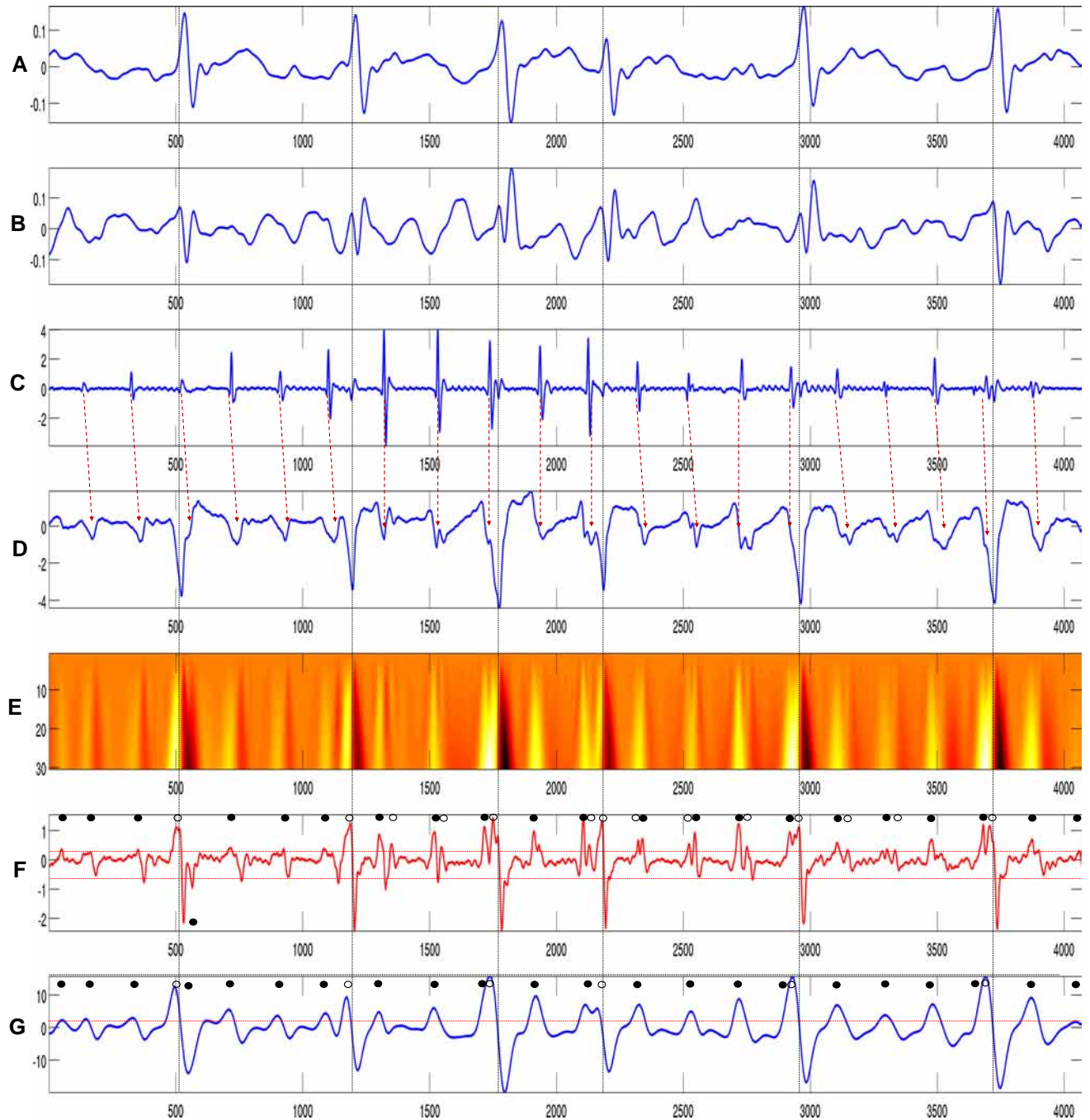
Fig. (3). The proposed wavelet analysis method was applied to the atrial electrograms at the site I in the LA anterior wall of a patient with PAF. (**A**) ECG I lead. (**B**) ECG aVF. Starting point of QRS event is denoted by dotted vertical lines. Atrial electrograms were collected by distal of ablation catheter (bipolar) and non-contact EnSite array (unipolar) simultaneously at the site I in (**C**) and (**D**), respectively. The scalogram for the unipolar electrogram using wavelet transforms was displayed in (**E**). Weighted fine and coarse scale electrograms f_{fine} and f_{coarse} were constructed in (**F**) and (**G**), respectively.

take advantage of the consistent concurrency between ventricular activities and waveform oscillations in surface ECG data. However, we argue subtracting QRS from original unipolar signals will lose some local information, which will be demonstrated later in this subsection. Here the ECG lead data will be used to detect the starting point of QRS event, denoted by a dotted vertical line in Fig. (**3**). Meanwhile, atrial electrograms were collected by distal of ablation catheter (bipolar) and non-contact EnSite array

(unipolar) simultaneously at the site I (in LA anterior wall) (Fig. **3C-D**). The dotted red lines demonstrate the related activation times between the two recording approaches, which is used to validate our results on unipolar electrogram using the wavelet filter.

The scalogram for the unipolar electrogram using wavelet transforms was displayed in Fig. (**3E**), and weighted fine and coarse scale electrograms f_{fine} and f_{coarse} were constructed in Fig. (**3F-G**) respectively. First, local maxima
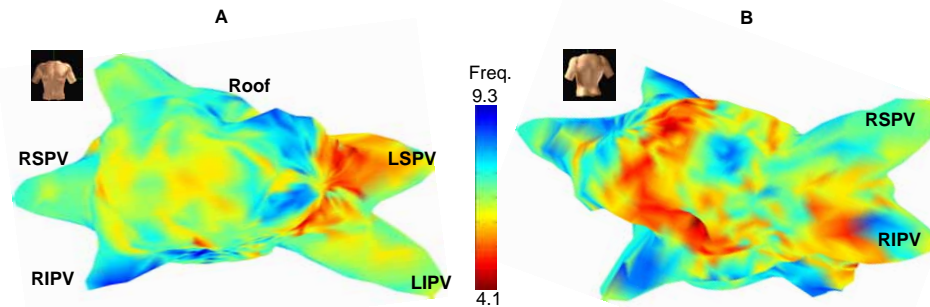
Fig. (4). Spatio-temporal activation patterns are displayed here, which presents serial snapshots of potentials reconstructed across the LA at the left postero-superior view over the period of 145 ms to 465 ms illustrated in Fig. (**3**). Preferential electrical pathways involving ridge/LSPV, atrial roof, PLA, atrial floor, MV and ASS were observed twice. Electrical activation started from ridge/LSPV region at ~145 ms, then it spread to atrial roof (165 ms), PLA (225 ms), atrial floor and MV (265 ms). A separate wave was initialized in ASS at ~305 ms and it quickly swept across the LA anterior wall to the LSPV. LAA = left atrial appendage; ASS = antero-superior septum; LSPV = left superior pulmonary vein; MV = mitral valve; PLA = posterior left atrium.

above surrounding data with a threshold value, where the derivative changes from the positive sign to negative, were detected (see peaks above the red dotted line in Fig. **3G**). Then the wavelet method was again used in fine scale electrograms f_{fine} to refine the initial results (Fig. **3F**). Within 90 ms to QRS (the vertical lines), if there is only one major positive and negative peaks (see the two dotted red horizontal lines), we consider that only QRS happened. Otherwise, it means LA was activated as well at the site *I* if there is double positive/negative peaks. The "true" activation times are indicated in black dots and QRS in white in Fig. (**3G**). In this typical example, our wavelet-based procedures correctly identify each of these wavefronts and reject fractionated potentials due to tortuous electrical propagation adjacent to the location I.

Finally, it was assumed that multiple events separated by < 90 ms reflect fractionated electrical activity and in this case the signal with greatest power in weighted coarse scale electrograms was selected as the principal activation. As indicated in Fig. (**3F**), fine scale electrograms f_{fine} provides an effective way to calculate fractionation of AF.

2.3. Tracking Electrical Activation Pathways

During PAF, electrical activation pathways may vary from beat to beat. How to quantify or even describe the pathways is a difficult problem. As a start, we use the same PAF patient data for illustration. Distinct spatio-temporal activation patterns are evident in Fig. (**4**), which presents serial snapshots of potentials reconstructed across the LA over the period of 145ms to 465ms displayed in Fig. (**4**). Firing of an automatic focus started from ridge/LSPV region at ~145 ms, then it spread to atrial roof (185 ms), PLA (225 ms), atrial floor and MV (265 ms). Next, a separate wave assuming from the right atrium (RA) was initialized in the antero-superior septum (ASS) at ~305 ms and it quickly swept across the LA anterior wall. Finally at ~385 ms it reached the ridge/LSPV region where it originally started. Different activation pattern was displayed from ~425 ms to ~465 ms. We can see that PLA and MV regions were not fully activated before ASS was depolarized.

In this study, we proposed to analyze the electrical activation pathways by examining the atrial electrograms in 2D problem instead of 3D considering it will be much easier to do computing directly on a regular 2D plane than a 3D atrial anatomical surface. This is how the EnSite array maps atrial electrograms from 8x8 recording catheters to the 2048 locations across the 3D LA endocardial surface (Fig. **1A**). Fig. (**5A**) gives the relation between the 2D plane with atrial anatomical structure for this patent's LA. Centroids of electrical activation wave-front ellipses were computed and saved at each snapshot as demonstrated in Fig. (**5B**). We processed the 4.1 s-long atrial electrograms at a step of 5 ms and occurrences of activation centroids were display in Fig. (**5C**). High occurrences indicate the atrial regions with either slow conduction or high frequency.

3. RESULTS

3.1. Activation Frequency Across LA

Employing the same procedure outlines in the 2.2 section for atrial unipolar electrograms on all 2048 sites on the LA, activation frequency values could be obtained. The frequency was superimposed on the 3D LA showing in different views in Fig. (**6**). The frequency in the LA of this patient with PAF varied from 4.1 to 9.3 Hz. Regions with activity in the upper quartile of frequencies were identified as high frequency. Multiple regions of high frequency electrical activity were seen in the patient: roof of the LA, the ASS, the PIS, two left PVs and RIPV. The computed frequency map is in line with 3D electrical propagation patterns, as well as clinical observations [7]. Extra care was taken to isolate these high frequency regions during ablation procedure. Computed frequency maps indicated lower frequency throughout atrial chambers post-ablation, which suggests the high frequency regions detected by our approach pre-ablation are the substrates/triggers of AF.

Regional AF frequency estimates were superimposed on 3D reconstructions of the LA for each of thirteen PAF patients. A connected region of high frequency activation spreads across the LA roof, ridge, and LSPV. High frequency
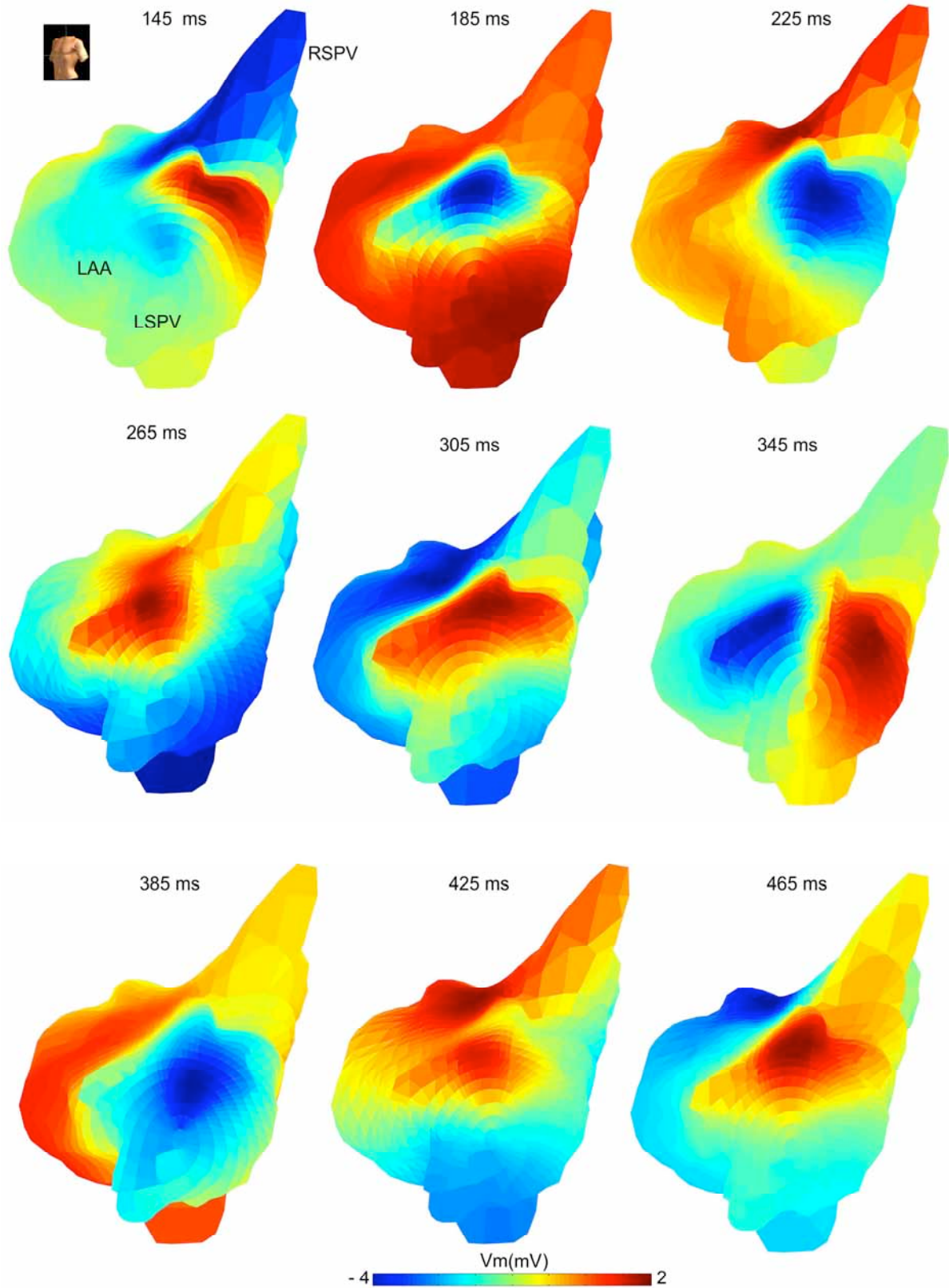
Fig. (5). Activation pathways of LA on 2D reconstruction of potentials for a patient with PAF. (**A**) The relation between the 2D plane with atrial anatomical structure for this patent's LA. (**B**) Centroids of electrical activation wave-front ellipses were computed and saved at each snapshot. (**C**) Occurrences of activation centroids during the 4.1 second recording time. (**D**) Schematic representation of electrical pathways in the LA. The colour spectrum displays occurrence of electrical activation. LAA = left atrial appendage; RLA = right lateral wall; LLW = left lateral wall; ASS = antero-superior septum; PIS = postero-inferior septum; LSPV = left superior pulmonary vein; LIPV = left inferior pulmonary vein; RSPV = right superior pulmonary vein; RIPV = right inferior pulmonary vein; MV = mitral valve. The ridge is the triangle region between the LA roof, LSPV and LAA. PLA = posterior left atrium.
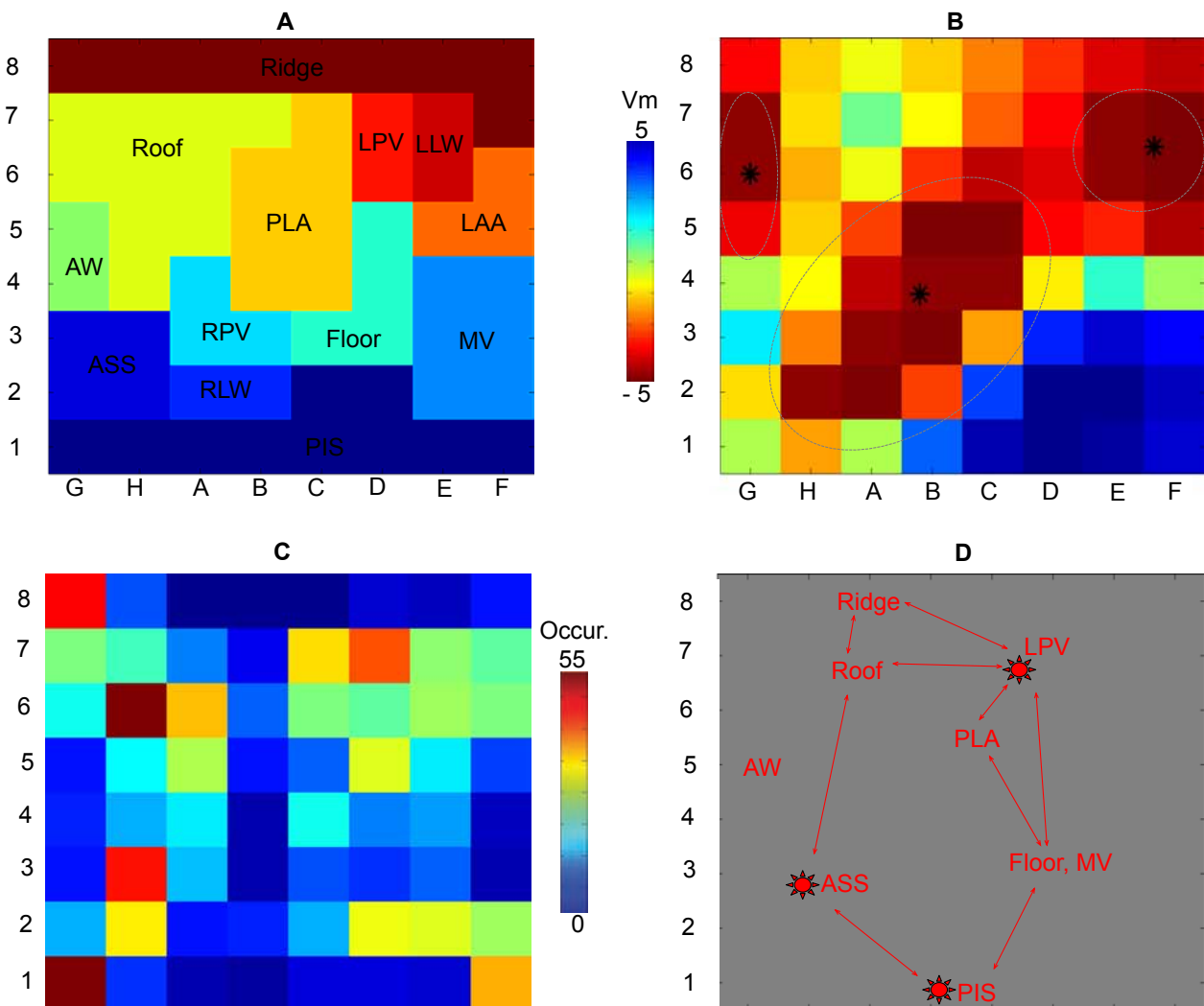
Fig. (6). Regional AF frequency estimates were superimposed on 3D reconstructions of the LA for the patient with PAF. Anterior and posterior views of a typical frequency map are presented in (**A**) and (**B**), respectively. The colour spectrum displays electrical activation frequency. LAA = left atrial appendage; RLA = right lateral wall; LLW = left lateral wall; ASS = antero-superior septum; PIS = postero-inferior septum; LSPV = left superior pulmonary vein; LIPV = left inferior pulmonary vein; RSPV = right superior pulmonary vein; RIPV = right inferior pulmonary vein; MV = mitral valve. The ridge is the triangle region between the LA roof, LSPV and LAA. PLA = posterior left atrium.

activity is also evident in the posterior inferior septum (PIS) and adjacent to antero-superior septum (ASS). The distribution of upper quartile frequencies for all 13 patients is represented in Fig. (**7**). Upper quartile frequencies were most commonly observed across the LSPV (10/12), ASS (9/13), PIS (9/13), ridge (8/13), and LIPV (7/13), whereas high frequency activity occurred much less often in the atrial floor (1/13).

3.2. Atrial Activation Pathways on LA During PAF

The 4.1 second-long atrial electrograms at a step of 5 ms were processed. At each time slot, centroids of electrical wavefronts were recorded and its overall occurrences were displayed in Fig. (**5C**). The regions with high occurrences are PIS, ASS, ridge, LSPV, LIPV, and atrial roof, which is consistent with Fig. (**6** and **7**). Fig. (**5D**) displays the schematic representation of electrical pathways in the LA and the red "sun" indicates the triggers of electrical activation. It detects a major macro circuit involving LPVs, PLA, atrial floor, MV, septum, atrial roof and ridge.

3.3. Catheter Ablation of PAF

Our group has achieved a 90.8 % success rate in treating PAF patients with a stepwise linear approach based on the roof line ablation [7], and observed the substrates of AF were mostly located in the roof, ridge, septum and left PVs areas. Here the ablation result is displayed in Fig. (**8**) for the same PAF patient used throughout this paper. PAF was converted to sinus rhythm around the LSPV region at the end points of catheter ablation with a stepwise linear approach based on the roof line ablation. It is a typical example, our recent clinical study suggests that ~80 PAF was terminated by Fig. (**7**) lesions (the RSPV-LSPV roof line plus the line along the ridge and both left PVs, ended at the MV).

4. DISCUSSION

4.1. Motivation

Nowadays, catheter ablation has proved to be a very effective approach in terminating PAF with ~80% success
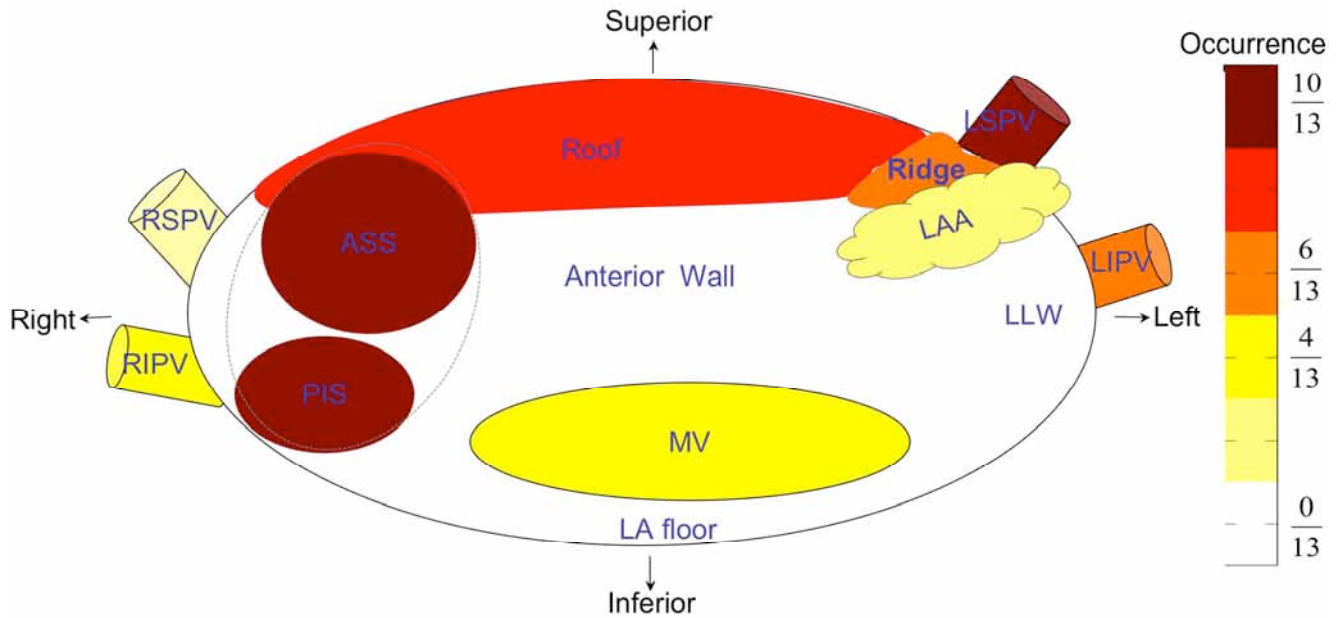
Fig. (7). Schematic representation of occurrence in the thirteen patients of upper quartile frequencies by region in the LA (the anterior view). The colour spectrum displays occurrence of electrical activation. LAA = left atrial appendage; RLA = right lateral wall; LLW = left lateral wall; ASS = antero-superior septum; PIS = postero-inferior septum; LSPV = left superior pulmonary vein; LIPV = left inferior pulmonary vein; RSPV = right superior pulmonary vein; RIPV = right inferior pulmonary vein; MV = mitral valve. The ridge is the triangle region between the LA roof, LSPV and LAA. PLA = posterior left atrium.
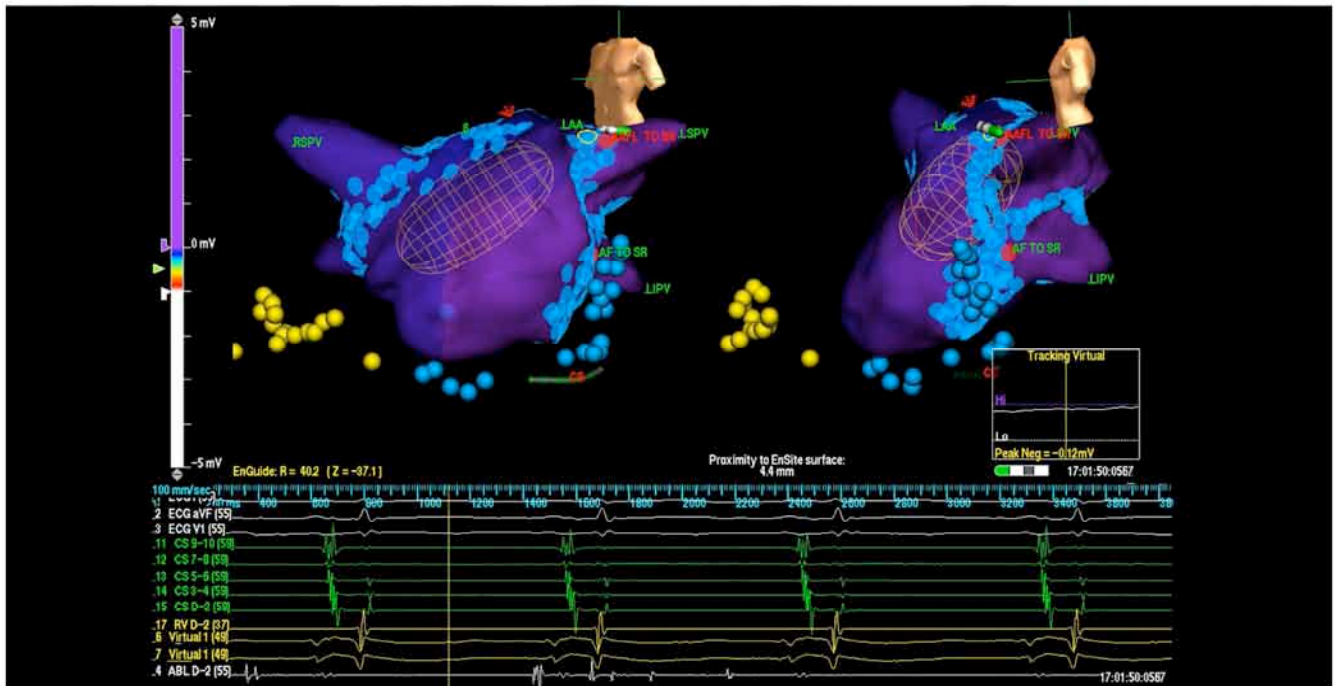
Fig. (8). PAF in the same patient in Fig. (**1** and **3**) was terminated around the LSPV region at the end of catheter ablation with a stepwise linear approach based on the roof line ablation.

rate, even though the success rate varies in different clinical centers [4]. However, in current practice different clinical centers employ different ablation strategies and tools. Circumferential PV isolation is the most common approach used for patients with PAF. Nademanee *et al.* [13] achieved a high success rate through targeting Complex Fractionated Atrial Electrograms (CFAEs). It has been demonstrated that LAA performed during AF may convert the AF to AT or flutter in approximately 10% of patients. Yao and his

colleagues [7] used stepwise linear ablation strategy as primary therapy and achieved 92.8% (142/153) success rate for PAF patients. This reflects differences among researchers in the exact mechanisms responsible for initiation and maintenance of PAF and how to terminate AF by catheter ablation. PAF is driven primarily by high frequency ectopic activity in the sleeves of the PVs [14, 15], which is the reason that PV isolation works in most cases. On the other hand, it indicates there exists some substrates beyond PVs.

We believe better understanding in substrate as well as triggers of fibrillation will lead to improve catheter ablation strategies for AF.

Despite recent advances in this area, current methods for identifying substrates in PAF all have shortcomings. Contact catheters are widely used for AF substrate identification, but this means that regions must be mapped sequentially in the presence of considerable spatial and temporal variability. The spectral analysis techniques most commonly employed for dominant frequency mapping [16-18] may not provide a complete characterization of short sequences of nonstationary time-series data [19]. The development of standardized criteria for defining CFAE regions has been problematic and identification of CFAEs remains subjective [20, 21]. Furthermore, CFAEs do not have a unique physical origin; they can be generated by nonuniform propagation, activation delays and wavefront collision.

It is evident that improved methods are needed for identifying substrates, electrical pathways and for assessing the effectiveness of ablation procedures in PAF [22]. Ideally, such techniques would provide real-time information across regions of the atria, especially the LA, that are sufficiently extensive to characterize 3D electrical activity reliably. Noncontact multi-electrode arrays offer a simultaneous view of 3D atrial electrical activity. Recently, there has growing tendency to perform catheter ablation in clinical settings with the aid of non-contact mapping system [23]. However, endocardial surface potentials recorded using this approach are unipolar signals and may provide less accurate estimates of dominant frequency than bipolar potentials recorded with closely spaced contact electrodes[3]. This work hopes to fill the gap.

4.2. Wavelet Based Analysis of Noncontact Atrial Electrograms

We have implemented signal processing techniques that enable regional activation frequency to be estimated at multiple 3D atrial sites from noncontact electrical mapping recordings. Our study indicates it is better not to remove the contribution of ventricular activation (QRS) before analysing atrial activation, otherwise it will lose some atrial activities. Wavelet decomposition method can separate atrial even from QRS, which is another advantage over other current widely employed methods (Fig. **3G**). However, the use of wavelet filtering to decompose reconstructed atrial electrograms into fine- and coarse-scale temporal events proved to be a critical step in objective classification of events within the reconstructed atrial electrograms. Houben *et al.* [24] used a very similar approach to separate local electrical events from far-field potentials in unipolar electrograms recorded on the epicardial surface of the RA. In their approach, an initial set of activation times was obtained by matching the electrograms with a library of 128 templates. The efficiency and effectiveness of the template matching are questionable. Instead, a simple and robust peak detection approach was developed for initial selection of activation events in our work. Furthermore, in this study, we have demonstrated that wavelet decomposition can also be used to separate the passage of activation wavefronts through a region from fractionated local activation. Activation wavefronts were associated with coincident local maxima in both weighted coarse- and fine-scale electrograms - that is events in which substantial depolarization were combined with a rapid increase in the rate of depolarization. On the other hand, maxima in weighted fine-scale electrograms only or secondary fine-scale maxima during coarse-scale depolarization were identified as fractionated events. The validity of this approach was established by bipolar electrogram recorded by distal of catheter ablation at the same site (Fig. **3**) and tracking the 3D spread of atrial activation through selected regions visually and comparing this with events classified by wavelet filtering of electrograms in those regions (see Fig. **4**). We have demonstrated that wavelet filtering provides a simple and highly robust means of identifying local activation in reconstructed atrial electrograms and also for extracting low amplitude fractionated activity from these data.

4.3. Electrical Activation Pathway Analysis

Reconstruction of electrical pathways in LA by tracking centroids of activation wave-front during AF (Fig. **5**) demonstrates it is a very promising approach. It detects a major macroreentrant circuit involving LPVs, PLA, atrial floor, MV, septum, atrial roof and ridge. The regions with high occurrences are septum, ridge, LSPV, LIPV, and atrial roof, which is consistent with the results using wavelet approach and our clinical observations. Our study strengthens the claim by Oral *et al.* [25] that both the PV and PLA are responsible for maintaining AF.

4.4. Implications for Catheter Ablation

The findings reported here are broadly consistent with recent clinical studies on the ablation of PAF. In this study, we have found that high frequency region are most commonly located in the atrial roof, two left PVs, ridge (bounded by LAA, LSPV and LA roof) and two septums (Fig. **7**). In contrast, high frequency activity was less common in the atrial floor. Yao and his coworkers noted that the lesions set on the ridge between the LAA and LPVs were most often involved in the termination of AF, both in paroxysmal and persistent AF. Termination of AF was achieved by linear ablation on the ridge area in 52.4% of patients. The Fig. (**7**) lesions (The RSPV-LSPV LA roof line plus the line along the ridge and LPVs ended at the MV) alone can achieve 77.1% (118 of 153) success rate of the PAF patients. It demonstrates that our approach could detect triggers/substrates of AF and guide catheter ablation. A typical example of the catheter ablation for the PAF patient is displayed in Fig. (**8**), AF was converted to sinus rhythm around the LSPV region at the end points of catheter ablation with a stepwise linear approach based on the roof line ablation. This study also showed that a linear ablation during an ongoing episode of AF can convert the majority of AFs to SR directly or at least to a more organized type of atrial tachyarrhythmia, i.e, atrial flutter. In this retrospective study, multiple, connected regions of high frequency activation were clearly observed in the same Patient LA, especially in LSPV, ridge, atrial roof (Fig. **6**), which explains why Fig. (**7**) lesions work so effectively for this PAF patient. Our preliminary results on twelve persistent AF (PeAF) using the wavelet approach indicate high frequency regions are located in atrial roof (11/12), ridge (9/12) and the two atrial septums (10/12). The difference in high frequency regions between

PAF and PeAF suggests that AF substrates have changed during the transition from PAF to PeAF, therefore, a different ablation strategy is needed for PeAF.

4.5. Limitations

Limitations of this study include the fact that the proposed method was performed in a small patient group with 13 patients in total, though the purpose of this paper is to develop and validate the novel approaches to characterize AF. As a result, it has not been possible to explore whether there is any change in the regional distribution of high frequency activity in the LA with duration of PAF. Furthermore, the "virtual" potentials obtained with noncontact electrical mapping are subject to error due to (i) imprecise reconstruction of the complex endocardial geometry of the LA, and (ii) aliasing as a result of the limited spatial sampling [23].

The wavelet-based analysis and wave-front centroid tracking used here proved to be robust and it has produced results that are repeatable and consistent with independent contact measurements made by our group and others during ablation of PAF. These limitations listed above defines future research planned by our group in this area, e.g., applying our approaches on a large data set of PeAF patients to understand mechanisms behind catheter ablation.

5. CONCLUSIONS

We have demonstrated that the application of wavelet-based analysis and wave-front centroid tracking to noncontact intra-cardiac mapping data provides a means of characterizing the spatiotemporal characteristics of LA electrical activity during PAF. The approach is robust, is sufficiently simple, computationally to be applied in real time and could therefore provide an efficient means of targeting potential substrates for AF. Regions of high frequency electrical activity in PAF identified in this study coincide with potential substrate/trigger targets identified by others for ablating PAF.

CONFLICT OF INTEREST

The authors confirm that this article content has no conflicts of interest.

ACKNOWLEDGMENT

REFERENCES

[1]   A.G. Brooks, M.K. Stiles, J. Laborderie, D.H. Lau, P. Kuklik, N.J. Shipp, L. Hsu, P. Sanders, "Outcomes of long-standing persistent atrial fibrillation ablation: a systematic review", *Heart Rhythm*, vol. 7, pp. 835-846, 2010.

[2]   L. Lo, S. Higa, Y. Lin, S. Chang, T. Tuan, Y. Hu, W. Tsai, H. Tsao, C. Tai, S. Ishigaki, A. Oyakawa, M. Maeda, K. Suenari, S. Chen, "The novel electrophysiology of complex fractionated atrial electrograms: insight from noncontact unipolar electrograms", *J. Cardiovasc. Electrophysiol.*, vol. 21, pp. 640-648, 2010.

[3]   J. NG, J.J. Goldberger, "Understanding and interpreting dominant frequency analysis of AF electrograms", *J. Cardiovasc. Electrophysiol.*, vol. 18, pp. 680-685, 2007.

[4]   R. Cappato, H. Calkins, S.-A. Chen, W. Davies, Y. Iesaka,J. Kalman, Y.-H. Kim, G. Klein, A. Natale, D. Packer, A. Skanes, F. Ambrogi, & E. Biganzoli, "Updated worldwide survey on the methods, efficacy, and safety of catheter ablation for human atrial fibrillation", *Circ. Arrhythm Electrophysiol.*, vol. 3, pp. 32-38, 2010.

[5]   G. Hindricks, H. Kottkamp, "Simultaneous noncontact mapping of left atrium in patients with paroxysmal atrial fibrillation", *Circ.*, vol. 104, pp. 297-303, 2001.

[6]   H. Takashima, K. Kumagai, N. Matsumoto, T. Yasuda, H. Nakashima, Y. Yamaguchi, S. Hida, S. Muraoka, C. Mitsutake, S. Miura, K. Saku, "Characteristics of the conduction of the left atrium in atrial fibrillation using non-contact mapping", *J. Cardiovasc.*, vol. 56, pp. 166-175, 2010.

[7]   Y. Yao, L. Zheng, S. Zhang, D. He, K. Zhang, M. Tang, K. Chen, J. Pu, F. Wang, X. Chen, "Stepwise linear approach to catheter ablation of atrial fibrillation", *Heart Rhythm*, vol. 4, pp. 1497-1504, 2007.

[8]   I. Daubechies, *"Ten Lectures on Wavelet"*. Philadelphia, PA: SIAM, 1992.

[9]   P.S. Addison, *"The illustrated wavelet transform handbook: Introductory theory and applications in science, engineering, medicine and finance"*, Taylor & Francis, New York, 2002.

[10]   P.S. Addison, "Wavelet transforms and the ECG: a review", *Physiol. Meas.* vol. 26, pp. 155-199, 2005.

[11]   P. Chang, J. Hsieh, J. Lin, F. Yeh, "Atrial fibrillation analysis based on blind source separation in 12-lead ECG data", ICMB, Springer-Verlag Berlin Heidelberg, 2010, pp. 286-295.

[12]   J.J. Rieta, F. Hornero, "Comparative study of methods for ventricular activity cancellation in atrial electrograms of atrial fibrillation", *Physiol. Meas.*, vol. 28, pp. 925-936, 2007.

[13]   K. Nademanee, E. Lockwood, N. Oketani, B. Gidney, "Catheter ablation of atrial fibrillation guided by complex fractionated atrial electrogram mapping of atrial fibrillation substrate", *J. Cardiovasc.*, vol. 55, pp. 1-12, 2010.

[14]   M. Haïssaguerre, M. Hocini, P. Sanders, F. Sacher, M. Rotter, Y. Takahashi, T. Rostock, L. Hsu, P. Bordachar, S. Reuter, R. Roudaut, J. Clementy, P. Jaïs, "Catheter ablation of long-lasting persistent atrial fibrillation: clinical outcome and mechanisms of subsequent arrhythmias", *J. Cardiovasc. Electrophysiol.*, vol. 16, pp. 1138-1147, 2005.

[15]   J. Zhao, T. Butters, H. Zhang, A. Pullan, I. LeGrice, G. Sands, B. Smaill, "An image-based model of atrial muscular architecture: Effects of structural anisotropy on electrical activation", *Circ. Arrhythmia Electrophysiol.*, vol. 5, pp. 361-370, 2012.

[16]   J.L. Salinet, A. Ahmad, P.D. Brown, P. Stafford, N.G. Andre, F.S. Schlindwein, *"Three-dimensional frequency mapping from the noncontact unipolar electrograms in atrial fibrillation"*, CinC, Hangzhou, China, 2010.

[17]   K. Yoshida, M. Ulfarsson, H. Oral, T. Crawford, E. Good, K. Jongnarangsin, F. Bogun, F. Pelosi, J. Jalife, Morady F, and A. Chugh, "Left atrial pressure and dominant frequency of atrial fibrillation in humans", *Heart Rhythm,* vol. 8, no. 2, pp. 181-187, 2011.

[18]   U. Richter, *"Spatial characterization and estimation of intracardiac propagation patterns during atrial fibrillation"*, Ph.D. thesis 2010, Lund University, Lund, Sweden.

[19]   M.R. Titchener, "Towards real-time measurement of information in a scientific setting", Communication Systems, Networks and Digital Signal Processing 2008, pp. 316-320.

[20]   H. Yamabe, K. Morihisa, J. Koyama, K. Enomoto, H. Kanazawa, H. Ogawa, "Analysis of the mechanisms initiating random wave propagation at the onset of atrial fibrillation using noncontact mapping: Role of complex fractionated electrogram region", *Heart Rhythm*, vol. 8, no. 8, pp. 1228-1236, 2011.

[21]   D. Katrisis, E. Giazitzoglou, D. Sougiannis, E. Voridis, S.S. Po, "Complex fractionated atrial electrograms at anatomic sites of ganglionated plexi in atrial fibrillation", *Europace*, vol. 11, pp. 308-315, 2009.

[22]   Y.K. Iwasaki, K. Nishida, T. Kato, S. Nattel, "Atrial fibrillation pathophysiology: Implications for management", *Circulation*, vol. 124, pp. 2264-2274, 2011.

[23]   M.J. Earley, D.J.R. Abrams, S.C. Sporton, R.J. Schilling, "Validation of the noncontact mapping system in the left atrium during permanent atrial fibrillation and sinus rhythm", *J. Am. Coll. Cardiovasc.*, vol. 48, pp. 485-491, 2006.

[24]   R.P.M. Houben, N.M.S.D. Groot, M.A. Allessie, "Analysis of fractionated atrial fibrillation electrograms by wavelet decomposition", *IEEE Trans. Biomed. Eng.*, vol. 57, no. 6, pp. 1388-1398, 2010.

[25]   H. Oral, C. Scharf, A. Chugh, B. Hall, P. Cheung, E. Good, S. Veerareddy, F. Jr Pelosi, F. Morady, "Catheter ablation for paroxysmal atrial fibrillation segmental pulmonary vein ostial ablation versus left atrial ablation", *Circulation*, vol. 108, pp. 2355-2360, 2003.